atmosphere

Article

Influence of Spatial Extraction Window Size on Wildfire Detection from MSG-SEVIRI Data Using Proper Orthogonal Decomposition

Muhammad Waqas [1], Leonardo Primavera [1,*], Giuseppe Ciardullo [1] and Valerio Tramutoli [2]

[1] Dipartimento di Fisica, Università della Calabria, Cubo 31/C, Ponte P. Bucci, 87036 Rende, CS, Italy; muhammad.waqas@unical.it (M.W.); giuseppe.ciardullo11@unical.it (G.C.)
[2] Dipartimento di Ingegneria, Università della Basilicata, Via dell'Ateneo Lucano, 10, 85100 Potenza, PZ, Italy; valerio.tramutoli@unibas.it
* Correspondence: leonardo.primavera@unical.it

Abstract

Wildfires represent a major environmental hazard with significant impacts on ecosystems, climate, biodiversity, and human activities. The increasing frequency and intensity of wildfire events have highlighted the need for reliable and timely detection techniques based on satellite remote sensing. This study investigates the application of Proper Orthogonal Decomposition (POD) to thermal observations acquired from the Spinning Enhanced Visible and Infrared Imager (SEVIRI) onboard the Meteosat Second Generation (MSG) satellite for wildfire anomaly detection. A wildfire event that occurred on 8 August 2021 in Calabria, Southern Italy, was selected as the primary case study. To assess the consistency of the POD response beyond the primary case, the analysis was further extended to two additional wildfire events, Viggianello–Abate and Pazzano–Montestella, using the 15 × 15 pixel extraction window. Middle Infrared (MIR, 3.9 μm) observations collected at 15 min intervals over a complete day were analyzed using four different spatial extraction windows (3 × 3, 15 × 15, 30 × 30, and 45 × 45 pixels). POD was employed to separate dominant background thermal variability from localized fire-induced anomalies. The analysis focused on higher-order POD modes, particularly the 6th, 7th, and 8th modes, which exhibited enhanced sensitivity to wildfire activity. Results showed that POD successfully identified thermal anomalies corresponding to wildfire occurrence times independently detected by the RST-FIRES methodology. The comparison of extraction window sizes revealed that the 15 × 15 pixel window provided the best balance between anomaly enhancement, spatial localization, and noise reduction. Larger windows introduced excessive spatial smoothing and reduced localization capability, whereas the smallest window was more affected by noise. The findings demonstrate the potential of POD as an effective complementary approach for wildfire detection and monitoring using geostationary satellite observations.

Keywords: wildfire detection; proper orthogonal decomposition (POD); remote sensing; MSG-SEVIRI; spatio-temporal analysis; middle infrared (MIR)

Academic Editors: Flavio T. Couto and Carolina Purificação

Received: 24 July 2026
Revised: 26 August 2026
Accepted: 28 August 2026
Published: 29 August 2026

1. Introduction

Wildfires are among the most destructive natural hazards affecting ecosystems, climate, biodiversity, and human society worldwide [1–5]. In recent decades, the frequency and intensity of wildfire events have increased significantly due to climate change, prolonged droughts, land-use changes, and anthropogenic activities [6–9]. These fires produce severe environmental and socio-economic impacts, including vegetation loss, atmospheric pollution, greenhouse gas emissions, and threats to human life and infrastructure [10–12]. Consequently, the development of reliable and rapid wildfire detection systems has become a major research priority in remote sensing and disaster management.

Satellite remote sensing has become one of the most effective approaches for wildfire detection and monitoring because of its capability to provide repetitive and synoptic observations over large geographic regions [13–17]. Polar-orbiting satellite sensors such as MODIS and VIIRS have been widely used for active fire detection owing to their relatively high spatial resolution and well-established fire products [14,15,18–20]. However, the temporal revisit period of polar-orbiting satellites is often insufficient for early wildfire detection and continuous monitoring of rapidly evolving fire events [21–23].

Geostationary satellites offer an important advantage for wildfire monitoring due to their high temporal resolution. The Spinning Enhanced Visible and Infrared Imager (SEVIRI) sensor onboard Meteosat Second Generation (MSG) provides observations every 15 min, enabling near real-time fire monitoring and improved detection of short-lived or rapidly developing fires. Previous studies demonstrated the potential of MSG-SEVIRI data for wildfire detection using contextual, threshold-based, and multi-temporal approaches [24–26]. In particular, the Robust Satellite Techniques for the FIRES (RST-FIRES) algorithm showed that multi-temporal analysis significantly improves the capability of detecting thermal anomalies associated with active fires.

Recently, advanced statistical and data-driven techniques have gained increasing attention in remote sensing applications for anomaly detection and feature extraction. Proper Orthogonal Decomposition (POD), also known as Principal Component Analysis in some contexts, is an efficient mathematical technique used to extract dominant spatial and temporal patterns from large datasets. POD has been successfully applied in environmental monitoring, fluid dynamics, meteorology, and remote sensing because of its capability to reduce dimensionality while preserving the most significant variability of the data [27–29]. In wildfire applications, POD-based methods can enhance thermal anomaly characterization by separating dominant background variability from fire-induced signals.

The method works by extracting a set of basis functions that are eigenmodes of the autocorrelation matrix of the field under study, integrated over the computational domain. These modes provide the largest energetic contribution to the original field. The method gives the distinction between long-lived structures of the temperature field and incoherent random fluctuations with sudden or persistent energetic structures, representing, in our case, the thermal anomaly field as a signature of the fire. However, given that the method is intrinsically statistical, the results depend on the dimension of the datasets. Maps of temperature fields spanning many pixels in both latitudinal and longitudinal coordinates can include many more sources of both background and random fluctuations, thus reducing wildfire detection performances. On the other hand, datasets involving a smaller number of pixels would decrease the statistical significance of the method, yielding poor statistical information. A trade-off is therefore necessary in order to obtain the best results from the method in terms of fire detection capabilities.

In this study, we carried out a systematic investigation of the POD applied to MSG-SEVIRI thermal observations of a single wildfire event, for which both the fire position and time are known, by using multiple extraction window sizes, including 3 × 3, 15 × 15, 30 × 30, and 45 × 45 pixels. By evaluating different spatial scales, this work aims to identify the influence of contextual information on wildfire anomaly extraction and to determine the most suitable extraction size for improved fire detection performance among those tested in this work. The proposed approach contributes to understand the scale-dependent thermal anomaly behavior in geostationary satellite imagery and provides new insights for operational wildfire monitoring systems.

2. Materials and Methods

2.1. Study Area and Wildfire Event

This study focuses on a single wildfire case located in Maierà (CS) [Grisolia]—Monte Romano, Calabria Region, Southern Italy. The wildfire event occurred on 8 August 2021 at approximately latitude 39.733138° N and longitude 15.842920° E. The selected event exhibited a clear thermal anomaly detectable in geostationary satellite observations and therefore represented a suitable case for testing the Proper Orthogonal Decomposition (POD) methodology for wildfire characterization.

To further evaluate the consistency of the POD response beyond the primary wildfire case used for the spatial-window sensitivity analysis, two additional wildfire events, Viggianello–Abate and Pazzano–Montestella, were examined. These events were treated as independent evaluation cases rather than being used to redefine the extraction window size. Based on the results obtained from the primary case, the 15 × 15 pixel extraction window was retained for these additional analyses, and the same POD procedure was applied to the corresponding daily MSG-SEVIRI MIR sequences. The temporal coefficients and spatial eigenfunctions of the intermediate POD modes were then examined for correspondence with the independently identified wildfire occurrence times and locations.

2.2. Satellite Data

The analysis was performed using observations acquired from the Meteosat Second Generation (MSG) satellite through the Spinning Enhanced Visible and Infrared Imager (SEVIRI) sensor. SEVIRI provides images every 15 min, allowing continuous monitoring of wildfire evolution in near real-time conditions.

Although SEVIRI includes multiple spectral channels, the present study exclusively employed Channel 04, corresponding to the Middle Infrared (MIR) band at 3.9 μm. This spectral region is highly sensitive to high-temperature targets and is widely used for active fire detection because burning surfaces emit strong thermal radiation in the MIR wavelength range.

For the selected wildfire event, a complete daily temporal sequence was collected. The dataset consisted of 96 temporal observations in the form of rectangular-shaped spatial maps of pixels, with each pixel containing the respective value of the brightness temperature, acquired at 15 min intervals, covering the period from 00:00 GMT to 23:45 GMT. The SEVIRI MIR Channel 04 has a nominal spatial sampling of approximately 3 km at the sub-satellite point, with the effective ground pixel size increasing with viewing angle away from the nadir. This spatial sampling sets the intrinsic localization scale of the analysis. Thermal anomalies associated with fires smaller than the pixel footprint may be spatially mixed with the surrounding background, reducing their apparent thermal contrast.

2.3. Data Preprocessing

The data analyzed in this study originated from MSG-SEVIRI Level 1.5 observations. Prior to each analysis, Channel 04 (3.9 μm) had already been extracted from the original dataset and provided as brightness-temperature fields. The input examined data consisted of binary arrays containing 32-bit floating-point brightness-temperature values in Kelvin. Likewise, no geometric, nor radiometric calibration is applied, since the spatial registration of the Level 1.5 observations had already been performed upstream. The SEVIRI MIR images report the measured brightness temperature on a large area spanning hundreds of kilometers. The first step of the analysis was to extract a spatial area around the wildfire location using different square extraction windows in order to evaluate the influence of spatial scale dimensions on thermal anomaly detection. The analyzed areas were selected by keeping the position of the fire in the center of the map. Four extraction sizes were considered:

- 3×3 pixels;
- 15×15 pixels;
- 30×30 pixels;
- 45×45 pixels.

For each extraction window, the temporal sequence of MIR observations was then analyzed through the POD technique and the results were compared in order to find out which window size yielded the best results in terms of fire detection. Notice that, in the analysis, we considered many more extraction windows (5×5, 10×10, 20×20, 60×60, to cite just a few), but we report here the results for the cases listed above because the others were very similar.

2.4. Proper Orthogonal Decomposition (POD)

Proper Orthogonal Decomposition (POD) was applied to the temporal sequence of SEVIRI MIR observations in order to extract the dominant spatial and temporal variability associated with the wildfire event. POD is a statistical decomposition technique that separates a dataset into orthogonal spatial modes and corresponding temporal coefficients.

The technique was used in the past to study the properties of the turbulence in channel flows [30,31], investigate solar coronal photospheric motions [32], or even for the medical detection of cancers [33]. More recently, it was also applied to detect the most energetic structures of the turbulence in tropical and tropical-like cyclones from several types of remote sensing satellite data [34–36].

The decomposition can be expressed as [28]:

$$T(x,y,t) = \sum_{k=1}^{N} a_k(t)\phi_k(x,y) \tag{1}$$

where $T(x,y,t)$ represents the spatio-temporal thermal field, $a_k(t)$ is the temporal coefficient, $\phi_k(x,y)$ is a set of orthogonal basis functions, and k denotes the POD mode number. The total number of modes, N, depends on how the basis functions are extracted. The basis functions are the solutions that maximize the time-average of the projection of the initial field on a generic function $\phi(x,y)$, namely:

$$\max \frac{\langle | < T, \phi > |^2 \rangle_t}{|\phi|^2}$$

where $\langle \cdot \rangle_t$ represents a time average and $< \cdot, \cdot >$ a scalar product in a suitable norm.

It turns out that the solution of this problem is not unique. There is a denumerable infinity of functions $\phi = \phi_k(x,y)$ that verify this property, and it can be found as the solution of the following Fredholm problem of the second kind:

$$\int_\Omega R(x,y,x',y')\,\phi(x',y')dx'\,dy' = \int_\Omega \langle T(x,y,t)T(x',y',t)\rangle_t\,\phi_k(x',y')\,dx'\,dy' = \lambda_k\,\phi_k(x,y) \tag{2}$$

where $R(x,y,x',y') = \langle T(x,y)\,T(x',y')\rangle_t$ is the autocorrelation tensor of the field under study (the brightness temperature, in this specific case) and Ω is the spatial domain (the rectangular map of pixels). This means that the solutions $\phi_k(x,y)$ are actually the eigenfunctions of problem (2). As usual, for a discrete sampling in both space and time of the fields, the number of eigenfunctions is not infinite, but rather equal to the number of analyzed snapshots of the field. Similarly, the continuous integrals can be transformed in discrete matrix operators and the problem is solved numerically.

Once problem (2) is solved and the discrete set of eigenvalues λ_k and eigenfunctions $\phi_k(x, y)$ are found, one can easily find the coefficient $a_k(t)$ of expansion (1) by projecting the original field on the corresponding basis function $\phi_k(x, t)$:

$$a_k(t) =< T(x, y, t), \phi_k(x, y) >$$

The POD eigenvalues, eigenfunctions and coefficients enjoy a series of remarkable properties [28]:

1. The eigenfunctions ϕ_k are orthonormal: $< \phi_l, \phi_m >= \delta_{lm}$;
2. The coefficients are uncorrelated on temporal average: $\langle a_l\, a_m \rangle_t = \lambda_m \delta_{lm}$;
3. From the two properties above, $\lambda_k = \langle |a_k|^2 \rangle_t$, that is, the k-th eigenvalue represents the "energy" (in temporal average) associated with the k-th eigenmode;
4. The time-average of the "energy" of the field equals the time-average of the coefficients: $\langle |T|^2 \rangle_t = \sum_k \langle |a_k(t)|^2 \rangle_t$;
5. The autocorrelation $R(x, y, x', y')$ can be written as:

$$R(x, y, x', y') = \sum_k \lambda_k\, \phi_k(x, y)\, \phi_k(x', y')$$

To summarize, there is a direct correlation between the POD modes and coefficients and the energetic content of the field. This can be interpreted by saying that the first POD mode retains the maximum energy of the field, the second retains the highest remaining energetic content, and so on. In conclusion, the first POD modes capture the bulk of the energy content of the field in such a way that even few POD modes are enough to describe the main characteristics of the field. Sometimes, this property is called the "optimality condition", in the sense that the POD spectrum is the one that captures the highest energy content of the field with the lowest number of modes (in other words, this means that the POD spectrum is the fastest to decrease as a function of the mode number).

Based on the previous considerations, it is understandable that the lower-order POD modes mainly describe the large-scale background variability (in the case of the daily temperature field, the diurnal thermal behavior), whereas intermediate-order modes isolate localized transient thermal anomalies related to wildfire activity. Finally, the highest-order modes describe less "coherent" thermal fluctuations or noise.

One advantage of the POD with respect to other decomposition methods (like Fourier or wavelet expansions) lies in the fact that no special requirement is imposed on boundary conditions, which can be completely generic. This means, for instance, that the method is fully scalable, in the sense that a large spatial domain area can be partitioned into smaller contiguous subdomains, and the POD is carried out on each of them independently. However, the method intrinsically depends on the size of the domain over which the decomposition is made. In particular, in the eigenvalue problem (2), the integral depends on the size of the spatial domain Ω, as well as the autocorrelation matrix $R(x, y, x', y')$. Such a dependency is related to the statistical nature of the method and, in particular, too large domains containing a large number of fluctuations having similar amplitudes. This could mask the contributions of the largest values. On the other hand, too small domains may enhance the contribution of even small fluctuations due to the poor statistics. Therefore, especially when the field consists of a global trend with superposed fluctuations and amplitudes comparable with one other (as is the case for the daily temperature field of wildfires). An analysis of the sensitivity of the results to the size of the domain has to be considered.

In this study, we performed such investigations on the sizes of the analysis domain to establish the best dimensions of the window containing the temperature field in order to better identify the local fluctuations of the temperature field connected to fire activity. In particular, we carried out the analysis on different window sizes (3 × 3, 15 × 15, 30 × 30 and 45 × 45 pixels, respectively) to see which one was more suitable for the identification of the fire from the temperature maps. Moreover, attention was given to the 6th, 7th, and 8th POD modes because these modes exhibited stronger sensitivity to fire-induced thermal perturbations.

2.5. Wildfire Detection Analysis

The temporal coefficients obtained from POD decomposition were analyzed to identify abnormal fluctuations associated with wildfire activity. The occurrence times of the detected anomalies were compared with the wildfire timing identified by the RST-FIRES methodology and documented fire in order to verify the consistency of the extracted thermal signals. Note that the results we use here concern the time and spatial localization of the fires obtained from databases and other algorithms. We do not intend to make any comparison of the effectiveness of the POD analysis with respect to other methods, but we simply want to show that our method yields results that are in perfect agreement with other kinds of analyses. Comparisons with other methods require a greater number of cases. Such an investigation is currently in progress and will be the subject of another article.

The spatial eigenfunctions associated with the higher-order POD modes were also examined to evaluate the spatial localization capability of each extraction window. The comparison among different extraction sizes allowed assessment of the trade-off between noise reduction, spatial smoothing, and wildfire localization performance.

The methodological workflow shown in Figure 1 and adopted in this study can be summarized as follows:

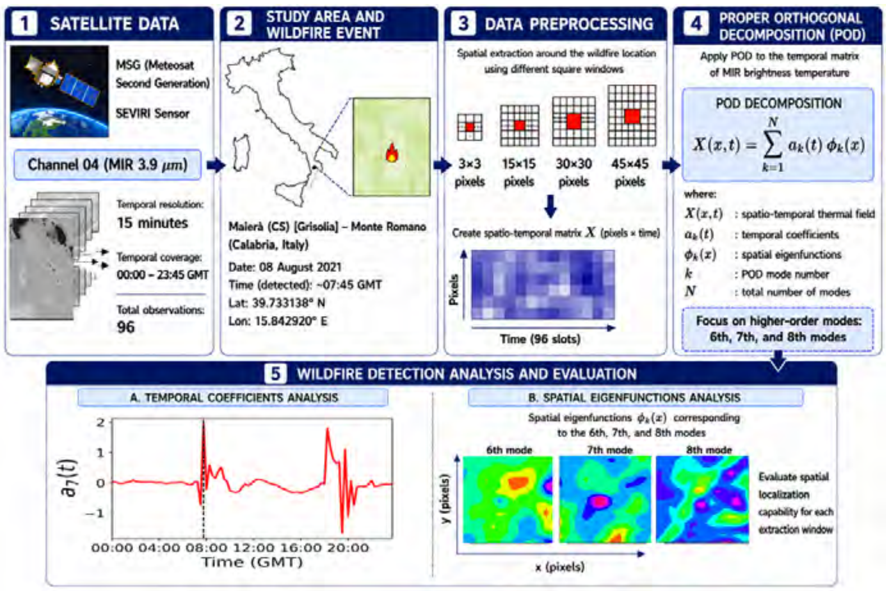

Figure 1. Systematic workflow of the proposed methodology for wildfire anomaly detection using MSG-SEVIRI Channel 04 and Proper Orthogonal Decomposition (POD).

1. Acquisition of MSG-SEVIRI MIR (3.9 μm) data for the selected wildfire event;
2. Spatial extraction around the wildfire location using multiple window sizes;
3. Construction of the temporal observation matrix;
4. Application of Proper Orthogonal Decomposition;
5. Analysis of temporal coefficients and spatial eigenfunctions for wildfire anomaly detection.

3. Results

Proper Orthogonal Decomposition (POD) analysis was applied to MSG-SEVIRI thermal observations using different spatial extraction windows of 3×3, 15×15, 30×30, and 45×45 pixels. The temporal coefficients $a_k(t)$ and the corresponding spatial eigenfunctions associated with the 6th, 7th, and 8th POD modes were analyzed in order to investigate their capability for wildfire detection and characterization.

The temporal domain considered in this study consists of 96 time slots corresponding to one complete day of MSG-SEVIRI observations acquired at 15-minute intervals. Therefore, the temporal sequence starts at 00:00 GMT and ends at 23:45 GMT. In this framework, time slot 0 corresponds to 00:00 GMT, time slot 1 corresponds to 00:15 GMT, and so on before ending at time slot 95, corresponding to 23:45 GMT.

The RST-FIRES algorithm detected fire activity at approximately 07:45 GMT, corresponding to time slot 31. This time is indicated by the dashed vertical lines in the temporal coefficient plots.

The POD decomposition revealed that the lower-order modes (0th–5th modes) mainly represent large-scale background variability and diurnal thermal behavior associated with solar illumination and land surface heating. In particular, the first two modes capture the dominant daytime thermal contribution caused by solar radiation and slowly varying atmospheric and surface conditions. Consequently, fire-induced thermal anomalies are not clearly distinguishable within these dominant modes because the wildfire signal remains masked by strong background energy contribution. Although the effective temperature associated with active combustion is substantially higher than that of the surrounding land surface, the brightness temperature measured by SEVIRI does not directly represent fire temperature because active burning generally occupies only a fraction of the satellite pixel. The measured MIR radiance therefore contains contributions from both the burning area and the non-burning background. Moreover, daytime solar heating and the reflected solar component in the 3.9 μm band can increase background variability and reduce the apparent fire-to-background contrast. The SEVIRI MIR channel saturates at approximately 335 K, further limiting the maximum measurable brightness temperature. Thus, weak or highly sub-pixel fires may produce only moderate departures from the surrounding thermal background.

In contrast, the higher-order modes, particularly the 6th, 7th, and 8th modes, exhibited clear transient perturbations associated with wildfire activity. These modes effectively isolate localized thermal anomalies from the dominant background variability and therefore provide a more sensitive representation of fire dynamics.

In our framework, the detection of the fire is carried out by looking at both the temporal evolution of the coefficients and the eigenfunctions. In particular, the coefficients of each single POD mode describe the time behavior of the temperature for the corresponding mode. Therefore, one should expect that, at the moment of the thermal anomaly induced by the fire, the coefficients should exhibit either a positive or negative peak. The corresponding eigenfunction, given the spatial distribution of the fluctuations, should instead show an either positive or negative peak corresponding to the position of the fire. In total, the (positive or negative) peak of the coefficients $a_k(t)$ for the modes 6, 7 and 8 should yield the time at which the fire is detected, while the (again, positive or negative) peak in the eigenfunction $\phi_k(x, y)$ should supply the information on the localization of the fire. Since this information was available from the RST-FIRES methodology, we selected the pixels of the spatial window for the given sizes in such a way that the fire position is always in proximity of the center of the window.

In the following figures, we show the results of our analysis by showing the behavior of the coefficients in time on the left, corresponding to the POD modes 6, 7 and 8, and the corresponding eigenfunctions as contour plots on the right. The detection of the fire is therefore carried out by looking at the presence of a peak in the coefficients, together with the presence of a peak (in both cases, the peaks can be either positive or negative) in the eigenfunction (identified, when found, as a red spot in the contour plots, falling in the middle of the shown area, since we chose this area as having the fire at the center). Furthermore, it should be noted that the values on the color bars corresponding to the eigenfunctions are only useful to establish the sign and intensity of the peak. According to Equation (1), the final value of the temperature is given by the product of the coefficient by the eigenfunction.

For the 3 × 3 pixel extraction shown in Figure 2, the temporal coefficients showed relatively noisy fluctuations due to the limited spatial context and reduced spatial averaging. Although some anomalies were visible near the fire occurrence times, the spatial eigenfunctions remained highly localized and fragmented, making fire identification less robust.

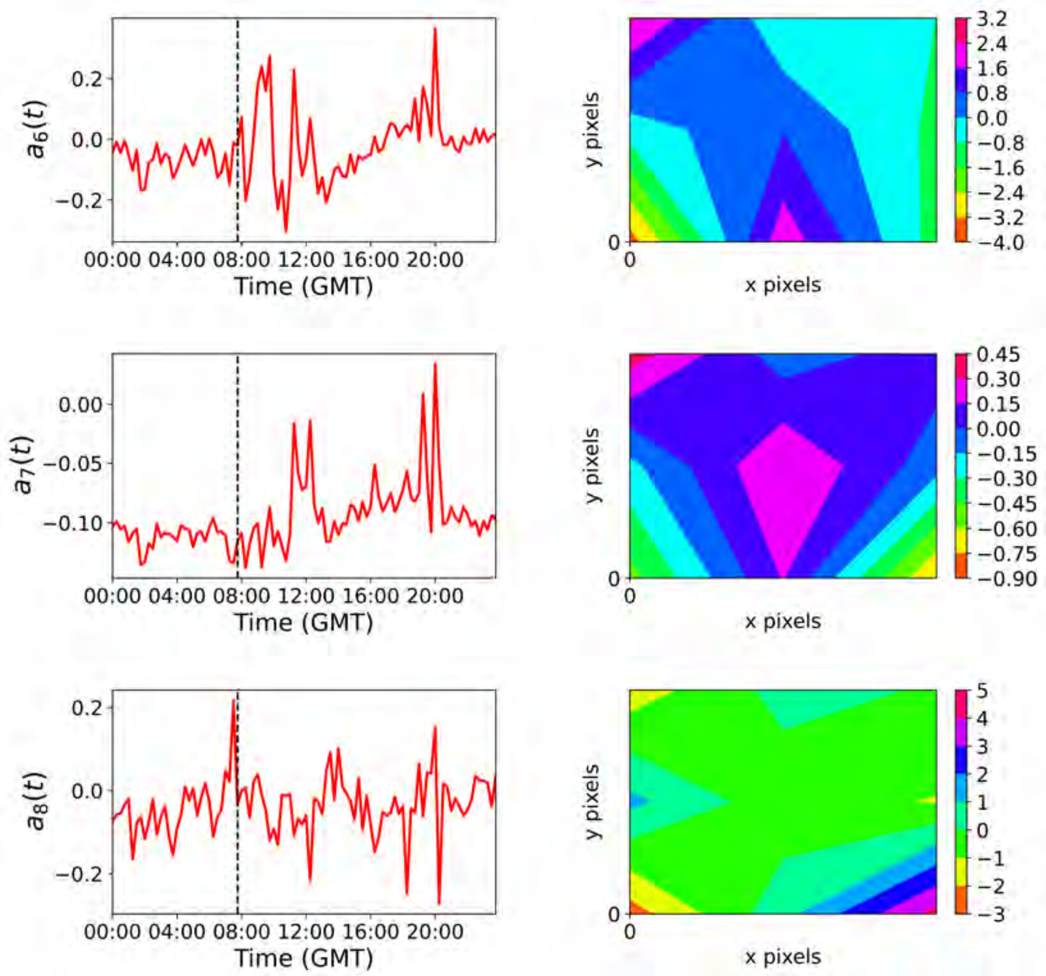

Figure 2. Temporal coefficients $a_k(t)$ and spatial eigenfunctions corresponding to the 6th, 7th, and 8th POD modes for the 3 × 3 pixel extraction window. In this plot and in all other similar plots, the dashed vertical lines indicate the wildfire occurrence times detected by the RST-FIRES algorithm at approximately 07:45 GMT and 09:15 GMT. Due to the limited spatial extent, the temporal coefficients exhibit relatively noisy fluctuations, while the spatial eigenfunctions remain highly localized and fragmented, reducing the robustness of fire identification.

To further examine the distribution of variability among the POD modes, the eigenvalue spectrum was evaluated for the 15 × 15 pixel extraction window of the Maierà (CS) [Grisolia]–Monte Romano event in Figure 3. The spectrum exhibits a pronounced decrease over the first few modes, indicating that most of the dominant variability of the thermal field is concentrated in the low-order POD components. The decay becomes progressively weaker at intermediate and higher orders, where individual modes represent substantially lower-energy contributions to the total thermal field.

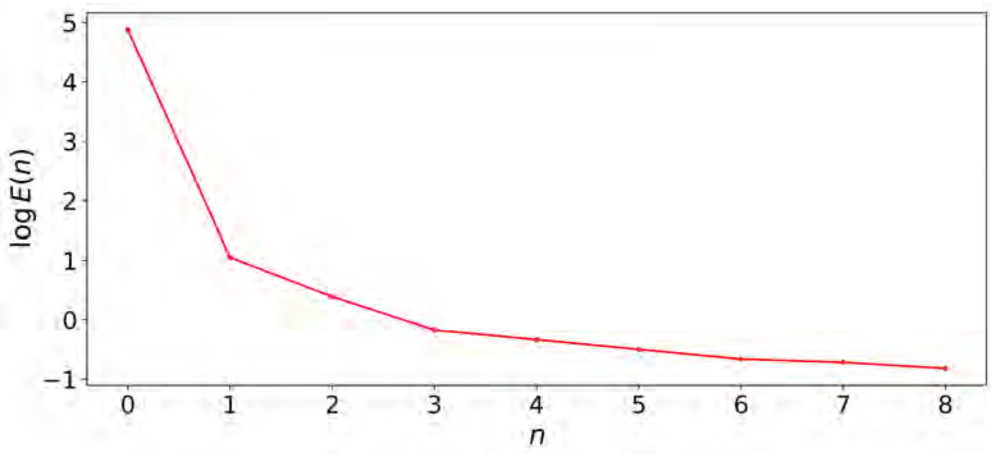

Figure 3. Eigenvalue spectrum obtained from the Proper Orthogonal Decomposition (POD) of the MSG-SEVIRI MIR (3.9 μm) brightness-temperature sequence for the Maierà (CS) [Grisolia]–Monte Romano wildfire using the 15×15 pixel extraction window. The logarithm of the POD eigenvalue, $\log E(n)$, is plotted as a function of mode order n. The spectrum shows a steep decrease for the first few modes, followed by a progressively flatter decay at higher orders, indicating the transition from dominant energetic structures to lower-energy components of the thermal field.

This behavior is consistent with the spatial and temporal characteristics of the POD decomposition. The dominant low-order modes primarily describe large-scale and persistent variations of the observed thermal field, including the diurnal evolution of land-surface temperature. Conversely, the lower-energy intermediate modes contain finer and more transient structures that are less dominant in the overall variance of the daily thermal sequence.

Importantly, the eigenvalue spectrum alone was not used as a sufficient criterion for identifying fire-sensitive modes. Mode selection was based on the combined examination of the eigenvalue distribution, the temporal coefficients $a_k(t)$, and the corresponding spatial eigenfunctions $\phi_k(x, y)$. In the present case, modes 6–8 were retained because their temporal coefficients exhibited perturbations associated with the independently identified fire period, and their spatial eigenfunctions showed localized structures within the wildfire region. The fact that the modes on which the fire is detected are not necessarily the most energetic ones can be understood while thinking that the eigenvalues represent the energy on a given POD mode, but rather are averaged in time (see the third property of the POD listed above). Since the fire itself is an energetic event (but, as explained before, the actual values of the temperature reached are not much higher than the daily changes) with a relatively short time duration, the energetic contribution, averaged over the 96 snapshots of the analysis, gives a modest contribution to the energy represented by the eigenvalues. Modes below this range were dominated by broader background variability, whereas progressively higher-order components showed increasingly weak and less coherent spatial fluctuations. Thus, the identification of modes 6–8 reflects both their position within the lower-energy part of the POD spectrum and their temporal and spatial correspondence with the wildfire event.

Another important point to be considered is that, although in our analysis the modes from 6th to 8th always show the signature of the fire, this is not necessarily the general case. Further analyses conducted on other case studies (with some of them shown below) show that the most meaningful modes can be different from the range 6–8. Again, what matters in fire detection is the presence of peaks in both the coefficient, at a given time, and in the eigenfunction, corresponding to the position of the fire. Everything else (order of POD modes, energetic content of the eigenvalues, and so on) is less significant in establishing the time and position of the fire.

The 15 × 15 pixel extraction, shown in Figure 4, provided the clearest and most distinguishable fire signature. The plot of the coefficient in time exhibits a very clear positive peak corresponding to time 07:45 (marked in the plots with the dashed vertical line) and the contour plots of the corresponding eigenfunctions show a clear positive (in red color) peak in the middle of the spatial domain. However, the thermal anomaly revealed by the peak in the eigenfunction $\phi_k(x, y)$ is more localized for modes 6 and 8 than for mode 7, for which it is spatially smoother and more distributed over the surrounding area. In addition to the fire-related peak, the temporal coefficients exhibit large fluctuations between approximately 18:00 and 23:00. These variations are attributed to the presence and movement of clouds over the study area, which introduces strong transient thermal variations that are captured by the POD decomposition but are unrelated to wildfire activity. In fact, what actually distinguishes the presence of a fire in the analysis is not the presence of a peak in the coefficients itself, but the contemporary presence of a peak in both the coefficient and eigenfunction; the two peaks must have the same sign in order for the final temperature at the point of the fire—that is, the product of two quantities—to have a maximum. In Figure 5, we validate this hypothesis by showing the total temperature field observed in an area around the fire at the times corresponding to the additional peaks observed in the coefficients. There is a clearly visible presence of clouds in the area, which lowers (instead of producing a maximum of) the temperature of the area surrounding the fire. Although the combined analysis of the POD temporal coefficients and spatial eigenfunctions allows cloud-induced perturbations to be distinguished from localized fire-related anomalies, some more information from additional SEVIRI spectral channels could be useful to identify and mask cloudy pixels before the POD analysis, thereby reducing cloud-related variability and the potential occurrence of false-positive detections. Furthermore, though the temporal coefficients still exhibited clear fluctuations near the time of fire occurrence, the spatial patterns indicated partial spreading of fire-related energy into neighboring regions.

The larger extraction windows of 30 × 30 and 45 × 45 pixels further increased spatial smoothing effects, as shown in Figures 6 and 7. In these cases, the POD modes captured broader regional variability, while the localized fire signatures became less concentrated. The temporal coefficients continued to show anomaly peaks during the fire period, particularly in the 6th and 7th modes, but the spatial eigenfunctions indicated a reduction in spatial sharpness due to the inclusion of large non-fire background areas. This behavior suggests that excessively large extraction windows may dilute the fire signal and reduce localization capability.

Overall, the analysis demonstrates that higher-order POD modes are more effective for wildfire detection because they suppress dominant background contributions and enhance localized transient thermal anomalies associated with active fires. Among the tested extraction sizes, the 15 × 15 pixel window provided the most suitable compromise between signal enhancement, spatial localization, and noise reduction. The results also confirm strong consistency between POD-derived anomalies and the fire occurrence times independently identified by the RST-FIRES methodology.

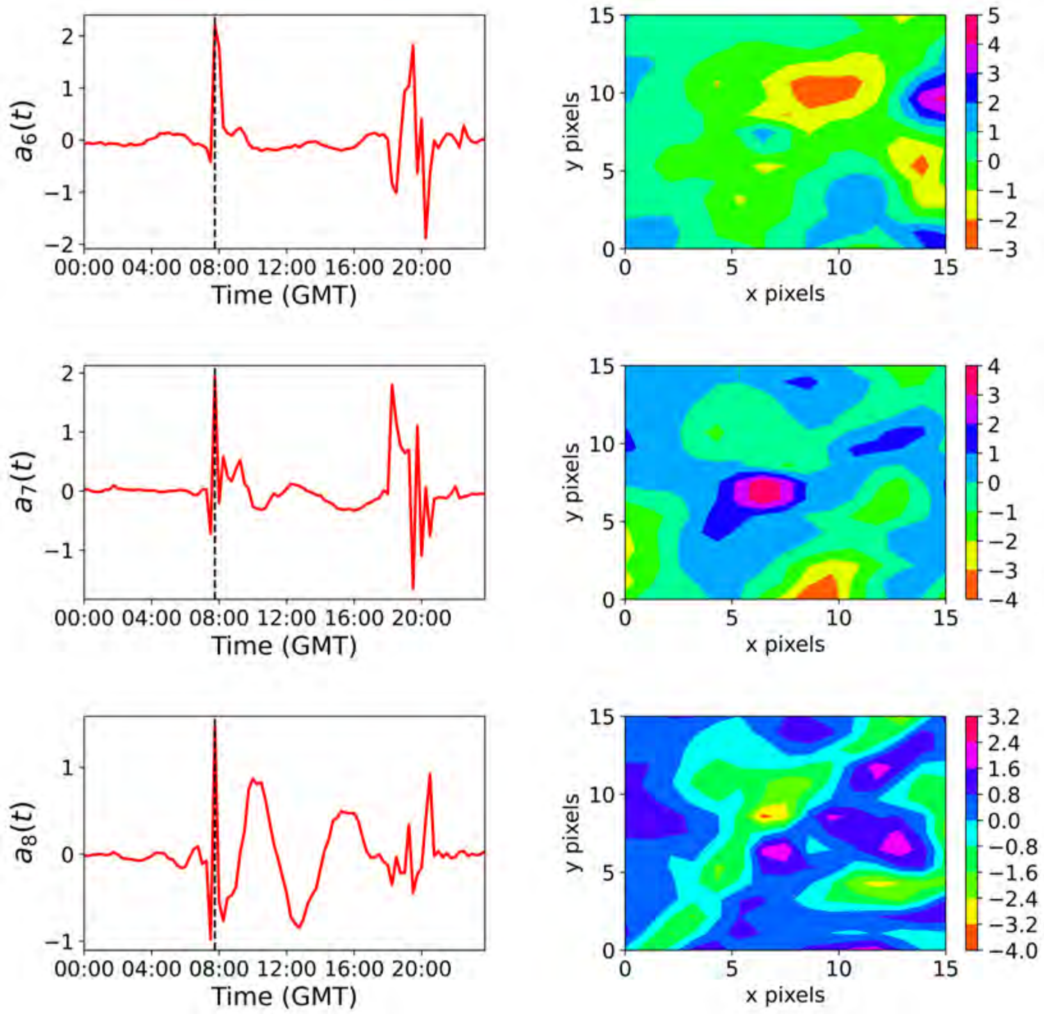

Figure 4. Temporal coefficients $a_k(t)$ and spatial eigenfunctions corresponding to the 6th, 7th, and 8th POD modes for the 15 × 15 pixel extraction window. Fire-related anomalies remain detectable in the temporal coefficients around the wildfire occurrence times; however, the spatial eigenfunctions exhibit smoother and more spatially distributed patterns, indicating partial spreading of the fire signal into the surrounding background regions.

To assess whether the POD behavior observed for the primary case was reproducible for independent wildfire events, the analysis was extended to the Viggianello–Abate and Pazzano–Montestella fires. Figures 8–11 refer to the Viggianello–Abate case study, while Figures 12–15 refer to the Pazzano–Montestella case.

For the Viggianello–Abate event in Figure 9, which refers to the 15 × 15 window size, the POD coefficients showed distinct temporal perturbations in the intermediate-order modes around the independently identified fire period. The corresponding spatial eigenfunctions also exhibited localized structures within the analysis domain. In particular, the behavior of the 6th and 7th modes demonstrates that the fire-related thermal variability is transferred from the dominant low-order background modes into intermediate modes where localized transient variability becomes more apparent. The response is not identical among the 6th, 7th, and 8th modes, indicating that the POD order associated with the clearest wildfire signature may vary between individual events.

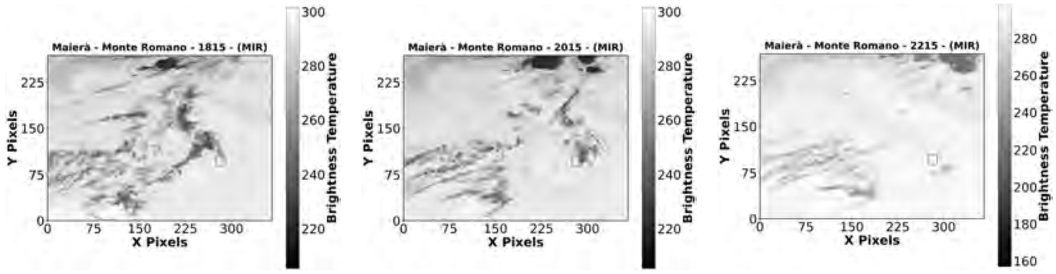

(**a**) 18:15 (**b**) 20:15 (**c**) 22:15

Figure 5. Evolution of the brightness temperature field over the study area at (**a**) 18:15, (**b**) 20:15, and (**c**) 22:15. The red rectangle indicates the 15 × 15 pixel region centered on the fire location and used for the POD analysis. The temporal evolution illustrates the movement of cloud structures across the study area, which produces transient variations in the POD temporal coefficients but does not correspond to a thermal maximum at the fire location.

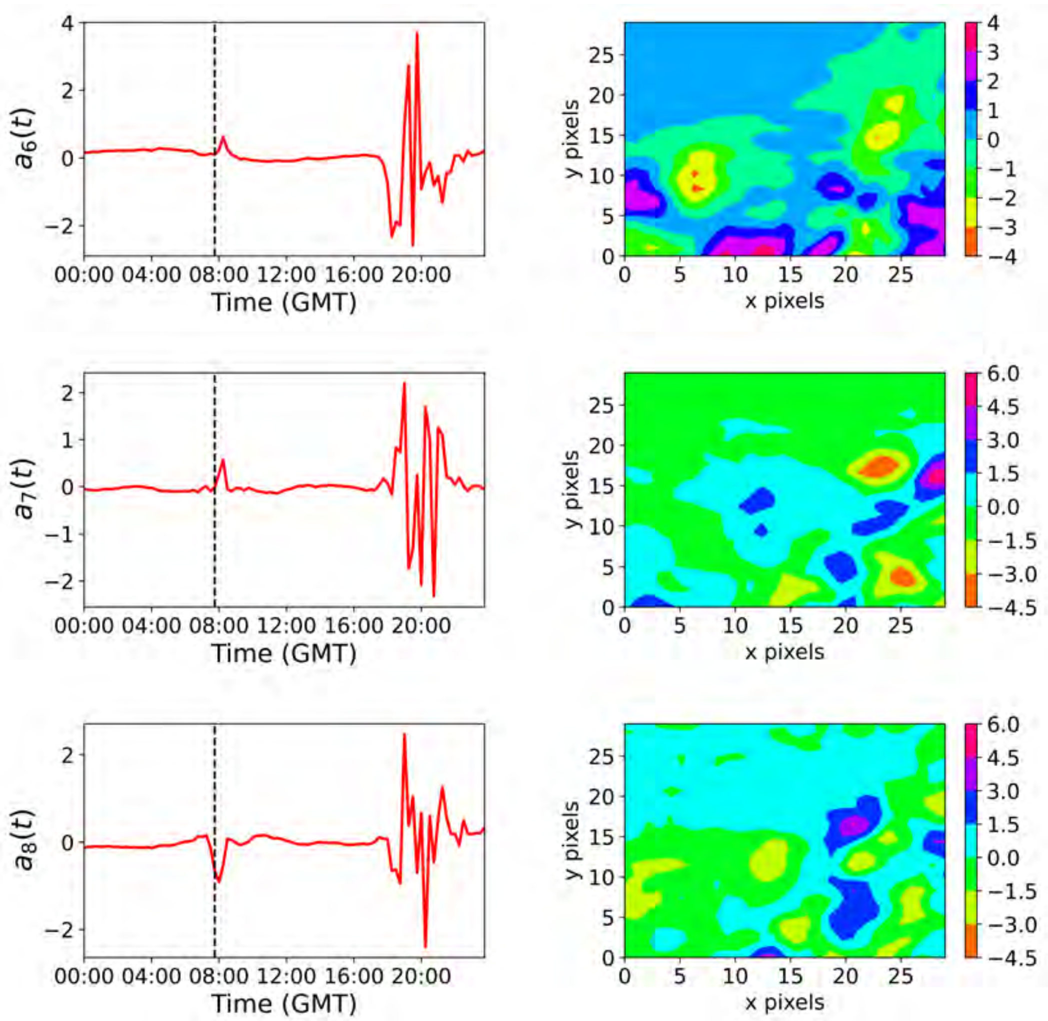

Figure 6. Temporal coefficients $a_k(t)$ and spatial eigenfunctions corresponding to the 6th, 7th, and 8th POD modes for the 30 × 30 pixel extraction window. The temporal coefficients continue to capture significant perturbations associated with wildfire activity, although the spatial eigenfunctions become increasingly influenced by broader regional variability. The larger extraction window introduces stronger spatial smoothing effects, reducing the sharpness of localized fire signatures.

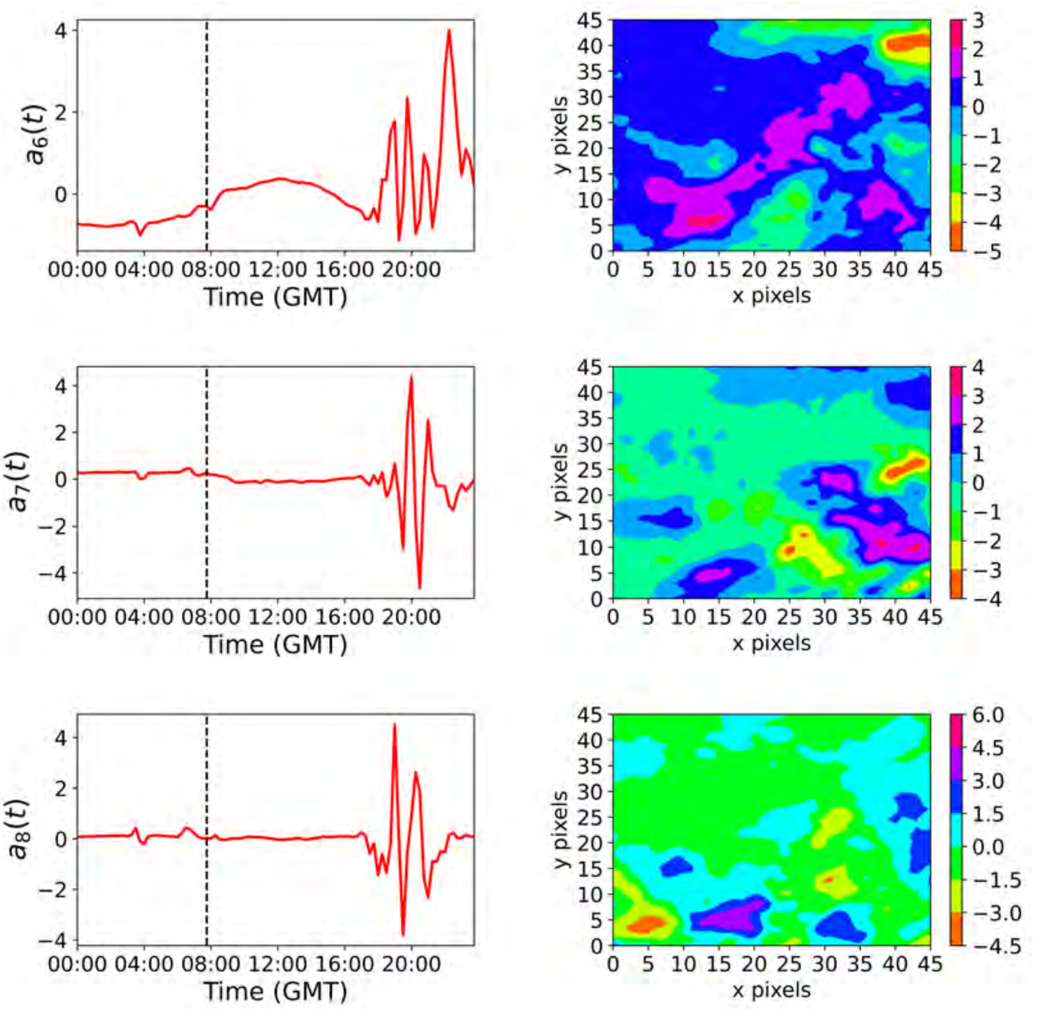

Figure 7. Temporal coefficients $a_k(t)$ and spatial eigenfunctions corresponding to the 6th, 7th, and 8th POD modes for the 45×45 pixel extraction window. While wildfire-induced anomalies are still observable in the higher-order temporal coefficients, the spatial eigenfunctions are dominated by large-scale background variability due to extensive spatial coverage. This behavior demonstrates that excessively large extraction windows may dilute localized thermal anomalies and decrease fire localization capability.

At the same time, for the Viggianello–Abate event, for window sizes of 3×3 and 45×45 (see Figures 8 and 11), there is no clear indication of a corresponding maximum or minimum in both the coefficients and eigenfunctions in all cases. This means, according to our criterion, that no detection of fire is possible with this method. However, in Figure 10, which refers to the case of a window size of 30 x 30, the fire detection is shown by the contemporary presence of peaks in both the coefficients and eigenfunctions for the POD mode $n = 8$. However, it should be noted that this is not in contrast with our statement: there is nothing preventing the possibility of fire detection with a different window size at 15×15 pixels. Simply, for all the cases studied until now, we found that the 15×15 window size yields the best results in terms of fire detection, while there is no special reason for which other window resolutions (as well as other POD modes with $n > 1$) cannot show the presence of fire.

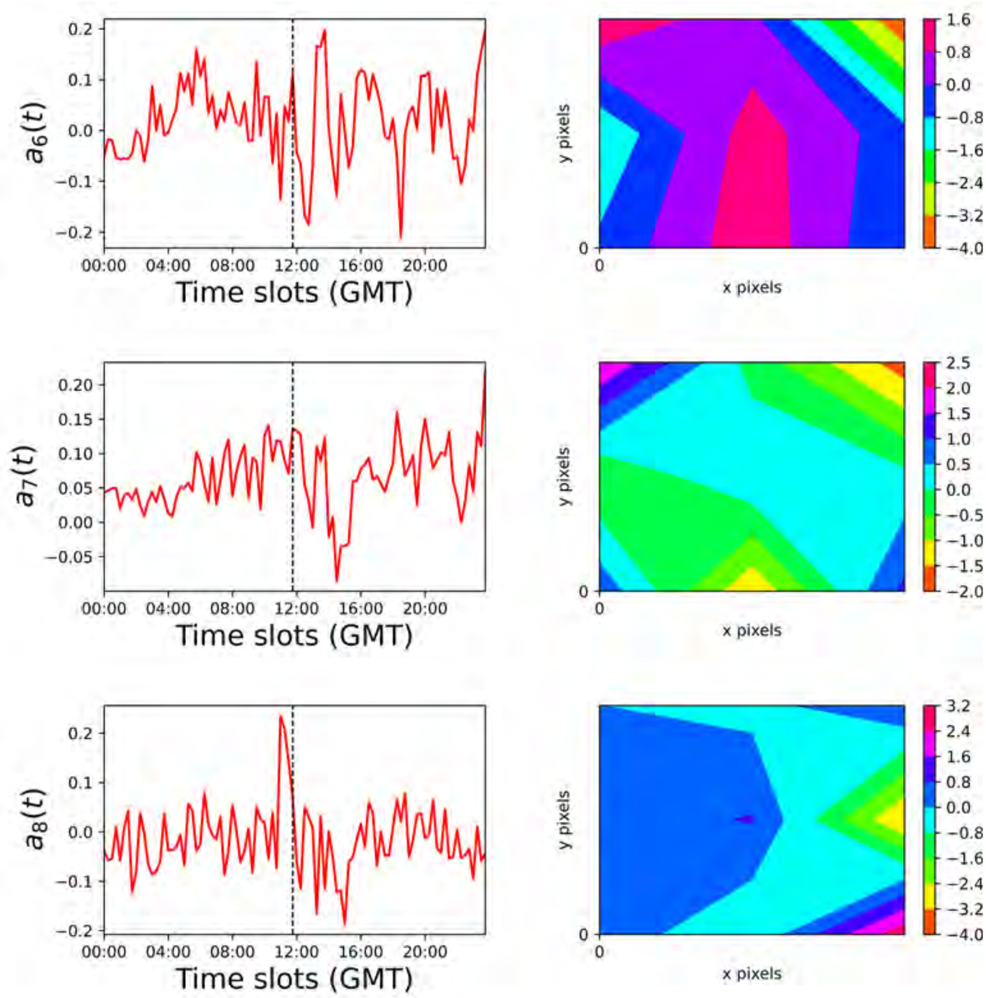

Figure 8. Temporal POD coefficients $a_k(t)$ (**left panels**) and corresponding spatial eigenfunctions $\phi_k(x, y)$ (**right panels**) for the 6th, 7th, and 8th modes obtained using the 3 × 3 pixel extraction window for the Viggianello–Abate wildfire event. The dashed vertical line indicates the independently identified wildfire occurrence time.

The Pazzano–Montestella event provides an additional illustration of this mode dependence in Figure 13. In this case, the 6th POD mode exhibits the clearest correspondence with the target wildfire, characterized by a pronounced temporal perturbation close to the independently identified occurrence time together with a spatially concentrated eigenfunction structure. This simultaneous temporal and spatial localization supports the attribution of the mode-6 perturbation to the Pazzano–Montestella thermal anomaly.

The 7th mode displays a different spatially localized structure that is not coincidental with the principal Pazzano–Montestella signature. Comparison with the available information for fires occurring during the same observation period indicates that this secondary feature is associated with the separate Placanica–Serre event. This result is noteworthy because POD is not constrained to represent only the target wildfire: when more than one sufficiently strong transient thermal anomaly occurs within the analyzed spatio-temporal field, their contributions may be distributed among different orthogonal modes. Consequently, the physical interpretation of individual POD modes should consider both the temporal coefficients and the spatial localization of the associated eigenfunctions.

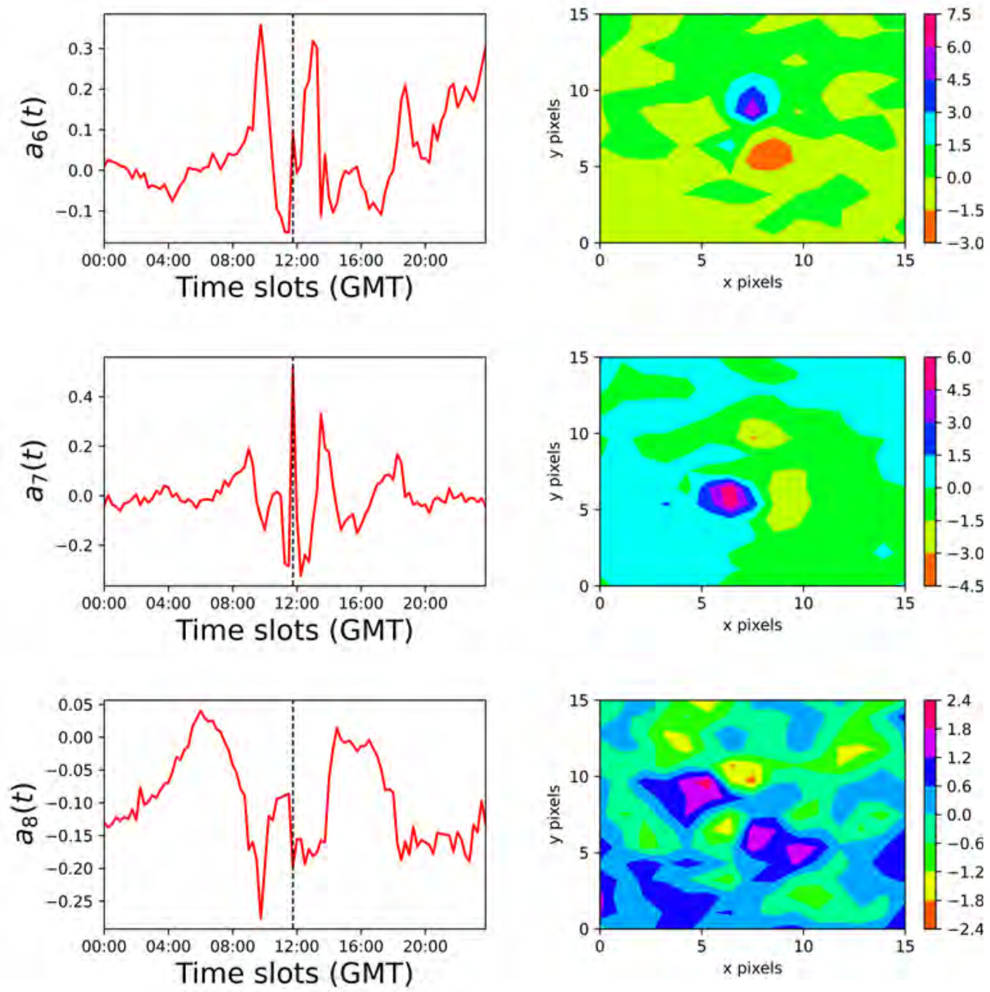

Figure 9. Temporal POD coefficients $a_k(t)$ (**left panels**) and corresponding spatial eigenfunctions $\phi_k(x, y)$ (**right panels**) for the 6th, 7th, and 8th modes obtained using the 15 × 15 pixel extraction window for the Viggianello–Abate wildfire event. The dashed vertical line indicates the independently identified wildfire occurrence time. The temporal coefficients show mode-dependent perturbations around the fire period, while the corresponding spatial eigenfunctions indicate the spatial organization of the thermal fluctuations within the extraction domain. The color bars represent the signed amplitude of the POD spatial eigenfunctions and do not correspond directly to brightness temperature.

In this case, in contrast with the Viggianello–Abate case , for all the resolutions—3 × 3 (Figure 12), 30 × 30 (Figure 14) and 45 × 45 (Figure 15)—there is no clear indication of the presence of fire in the sense that even when there is a peak in the coefficient of some mode, like in the case of mode $n = 8$ for the window size of 30 × 30, there is no corresponding peak into the contour plot of the eigenfunction.

Taken together with the primary wildfire analysis, the two additional cases indicate that wildfire-related thermal perturbations can consistently emerge within intermediate POD modes when the 15 × 15 pixel analysis domain is used. However, the mode containing the clearest fire signature is not necessarily identical for every event. The results therefore support the use of a range of intermediate modes rather than the assumption that a single fixed POD order will universally represent wildfire activity. Likewise, the additional cases strengthen the evidence that the 15 × 15 pixel configuration is suitable for the events examined here, while not establishing this window as universally optimal for all wildfire, surface, or atmospheric conditions. These findings indicate that POD analysis can effectively complement multi-temporal wildfire detection approaches using MSG-SEVIRI data, particularly when appropriate spatial extraction scales are employed.

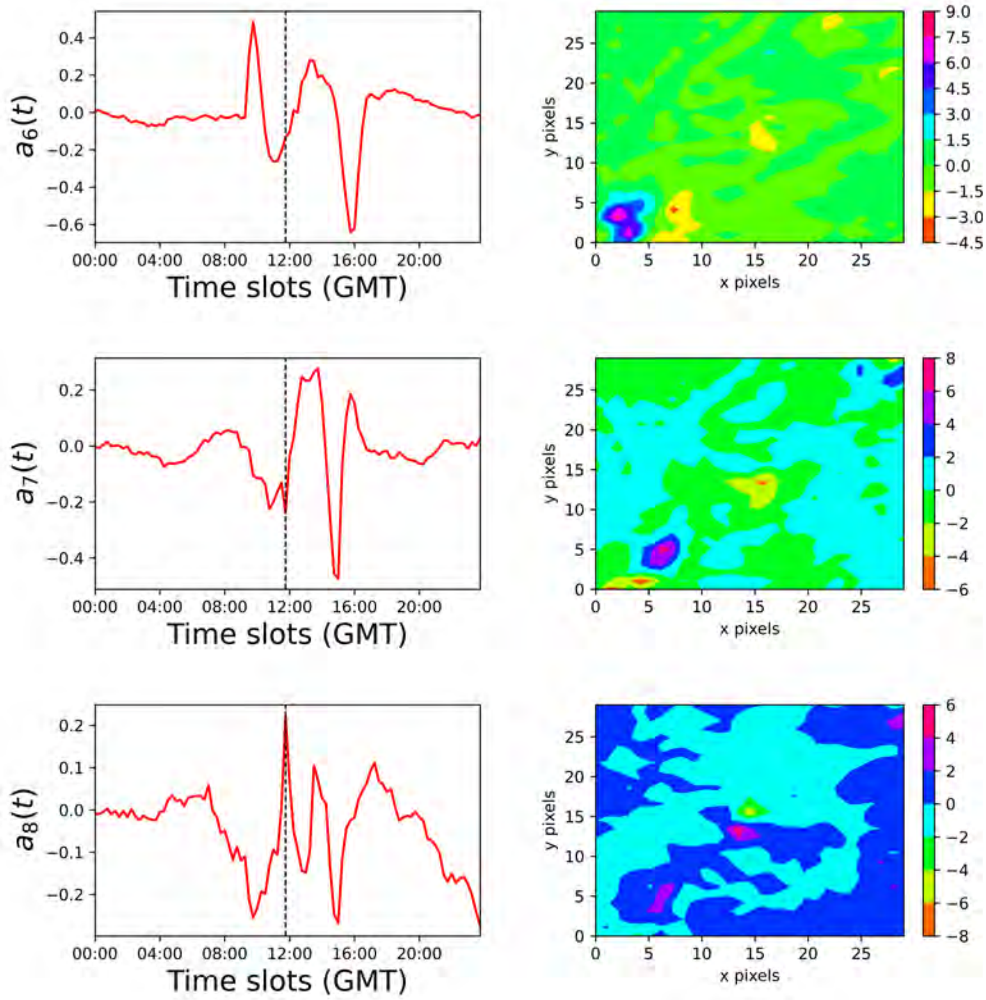

Figure 10. Temporal POD coefficients $a_k(t)$ (**left panels**) and corresponding spatial eigenfunctions $\phi_k(x, y)$ (**right panels**) for the 6th, 7th, and 8th modes obtained using the 30 × 30 pixel extraction window for the Viggianello–Abate wildfire event. The dashed vertical line indicates the independently identified wildfire occurrence time.

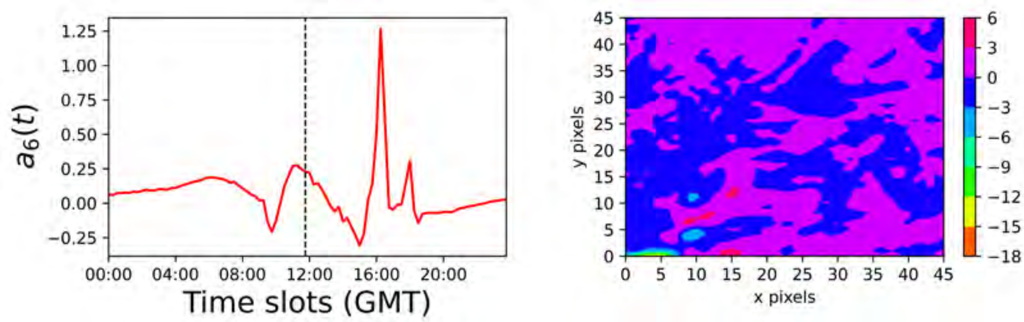

Figure 11. *Cont.*

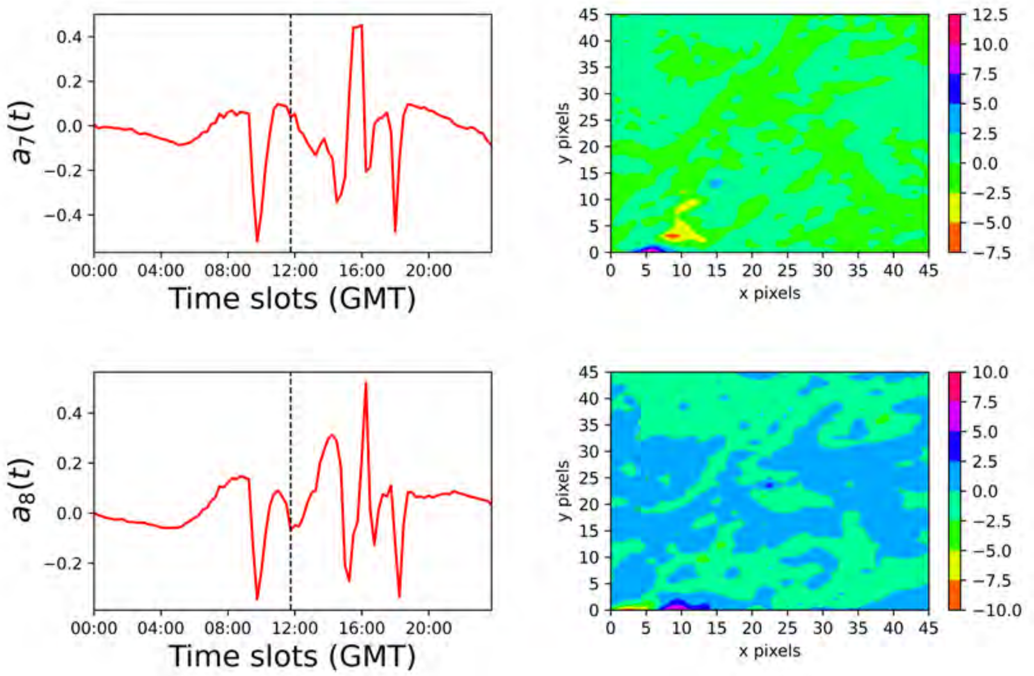

Figure 11. Temporal POD coefficients $a_k(t)$ (**left panels**) and corresponding spatial eigenfunctions $\phi_k(x, y)$ (**right panels**) for the 6th, 7th, and 8th modes obtained using the 45 × 45 pixel extraction window for the Viggianello–Abate wildfire event. The dashed vertical line indicates the independently identified wildfire occurrence time.

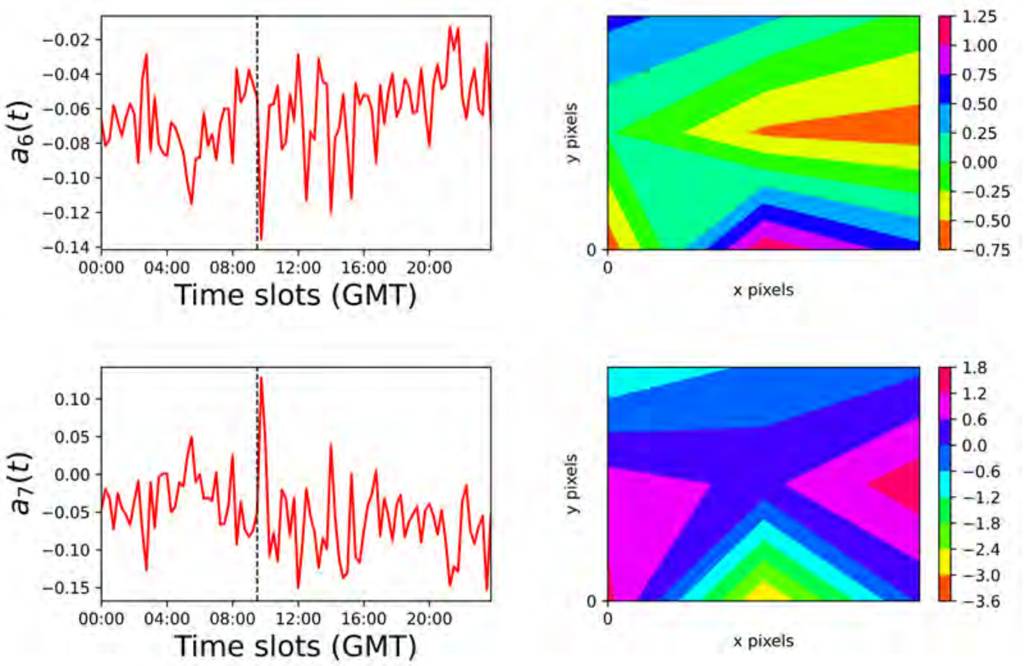

Figure 12. *Cont.*

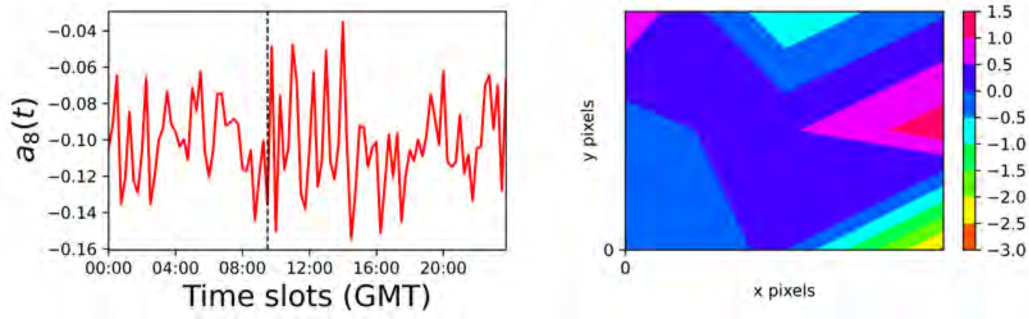

Figure 12. Temporal POD coefficients $a_k(t)$ (**left panels**) and corresponding spatial eigenfunctions $\phi_k(x, y)$ (**right panels**) for the 6th, 7th, and 8th modes obtained using the 3 × 3 pixel extraction window for the Pazzano–Montestella wildfire event. The dashed vertical line indicates the independently identified occurrence time of the Pazzano–Montestella fire.

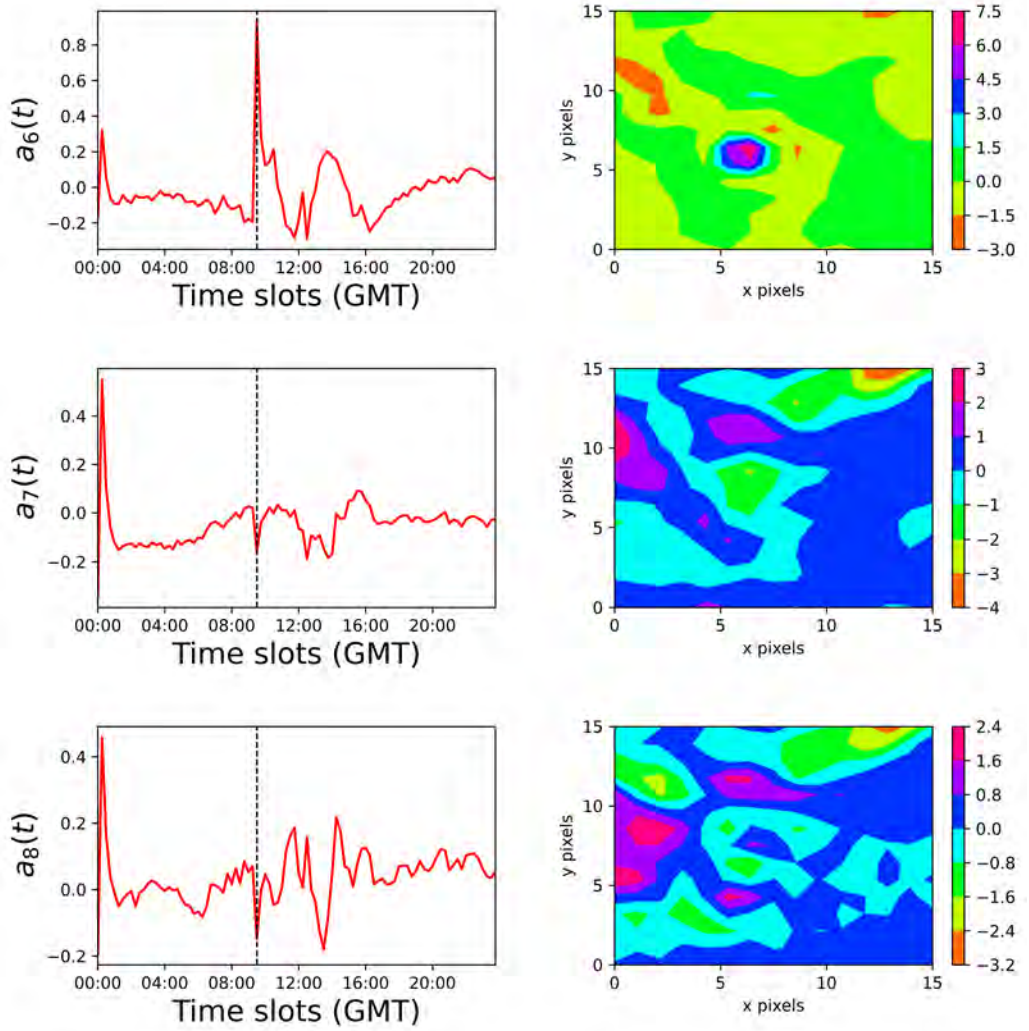

Figure 13. Temporal POD coefficients $a_k(t)$ (**left panels**) and corresponding spatial eigenfunctions $\phi_k(x, y)$ (**right panels**) for the 6th, 7th, and 8th modes obtained using the 15 × 15 pixel extraction window for the Pazzano–Montestella wildfire event. The dashed vertical line indicates the independently identified occurrence time of the Pazzano–Montestella fire. A pronounced temporal perturbation and a spatially localized eigenfunction structure are evident in the 6th mode around the target fire period. The 7th mode contains a spatially distinct anomaly interpreted in association with the separate Placanica–Serre fire occurring during the same observation period. The color bars represent the signed amplitude of the POD spatial eigenfunctions and do not correspond directly to brightness temperature.

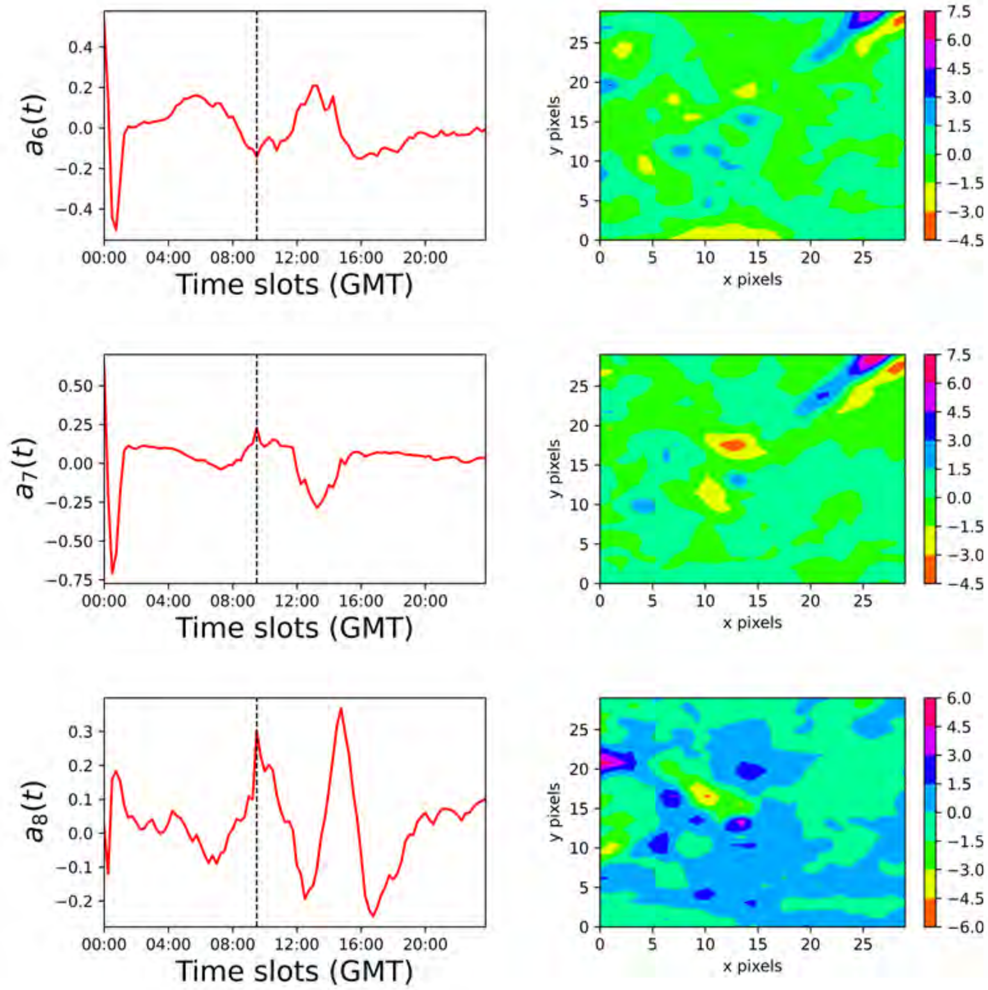

Figure 14. Temporal POD coefficients $a_k(t)$ (**left panels**) and corresponding spatial eigenfunctions $\phi_k(x, y)$ (**right panels**) for the 6th, 7th, and 8th modes obtained using the 30 × 30 pixel extraction window for the Pazzano–Montestella wildfire event. The dashed vertical line indicates the independently identified occurrence time of the Pazzano–Montestella fire.

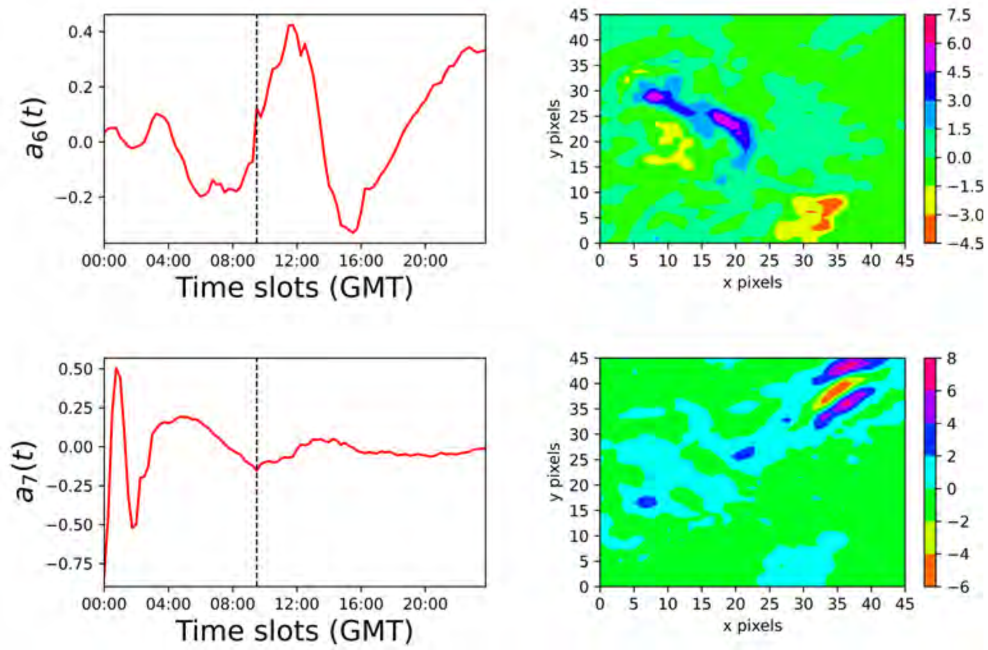

Figure 15. *Cont.*

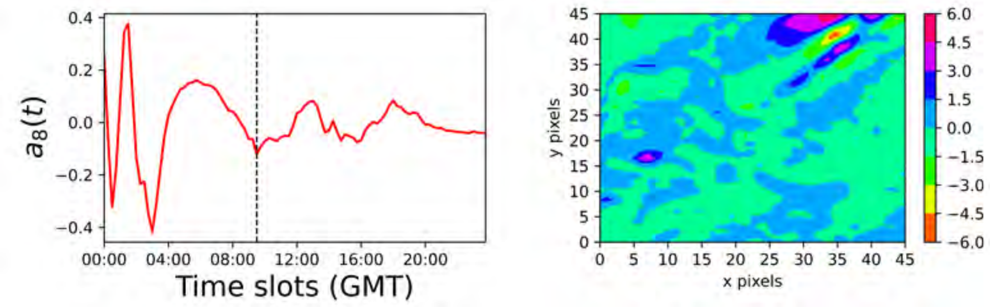

Figure 15. Temporal POD coefficients $a_k(t)$ (**left panels**) and corresponding spatial eigenfunctions $\phi_k(x, y)$ (**right panels**) for the 6th, 7th, and 8th modes obtained using the 45 × 45 pixel extraction window for the Pazzano–Montestella wildfire event. The dashed vertical line indicates the independently identified occurrence time of the Pazzano–Montestella fire.

4. Conclusions

This study investigated the capability of Proper Orthogonal Decomposition (POD) to detect and characterize wildfire-induced thermal anomalies in MSG-SEVIRI Middle Infrared observations and assessed the influence of different spatial extraction window sizes on detection performance. The results demonstrated that higher-order POD modes effectively isolate localized thermal anomalies associated with active fires by suppressing dominant background variability related to diurnal heating and large-scale environmental conditions.

A systematic comparison of four extraction windows (3 × 3, 15 × 15, 30 × 30, and 45 × 45 pixels) revealed a strong dependence of wildfire characterization on the selected spatial scale. The smallest window preserved spatial detail but exhibited increased noise and reduced robustness, while larger windows introduced substantial spatial smoothing and incorporated broader background variability, leading to a loss of fire localization capability. Among the tested configurations, the 15 × 15 pixel extraction window provided the best compromise between signal enhancement, noise reduction, and accurate spatial representation of wildfire activity.

As previously specified, the size of the window of pixels is not sufficient alone to determine the effectiveness of the method, in the sense that the spatial resolution of the single pixel is also relevant for the fire identification. However, for all the cases studied in this work, the resolution was always the one characteristic of SEVIRI. Therefore, it is not necessary to specify it. However, if the dataset involved also data from other satellites, the results could be different.

The temporal coefficients associated with the 6th, 7th, and 8th POD modes showed clear perturbations during the wildfire event and were consistent with fire occurrence times independently identified by the RST-FIRES algorithm. These results confirm that POD can effectively enhance wildfire-related signals in geostationary satellite observations and provide valuable information for operational fire monitoring systems.

One peculiar characteristic of the method is that it does not require any special hypothesis on the behavior of the dataset on the boundaries. This means that even a large area of pixels can be partitioned into sub-windows of size 15 × 15 (the best window size, according to the results obtained so far) and analyzed independently from the other. A peak in the coefficients and eigenfunctions in any sub-window corresponds to fire detection. This suggests the idea that the method could perhaps be used as a nowcasting tool for fires to detect the presence of a fire by analyzing a dataset of 24 h before the current time in any sub-window. However, this possibility cannot be stated by the simple analysis presented here and requires a much deeper exploration for confirmation. Further investigations of this possibility are in progress and will be the subject of a forthcoming paper.

Future work should extend the analysis to a larger number of wildfire events and different environmental conditions, and it should exploit additional SEVIRI spectral channels to implement cloud screening and reduce cloud-related false-positive detections. Furthermore, integrating POD with established wildfire detection algorithms and machine learning approaches may further improve the accuracy, robustness, and operational applicability of satellite-based wildfire monitoring systems.

Author Contributions: Conceptualization, M.W. and L.P.; methodology, L.P.; software, M.W. and G.C.; validation, M.W., L.P., G.C. and V.T.; formal analysis, M.W. and L.P.; investigation, M.W., L.P. and G.C.; resources, M.W., G.C. and V.T.; data curation, M.W., G.C. and V.T.; writing—original draft preparation, M.W. and L.P.; writing—review and editing, M.W., L.P., G.C. and V.T.; visualization, M.W.; supervision, L.P. and V.T.; project administration, L.P. and V.T.; funding acquisition, L.P. All authors have read and agreed to the published version of the manuscript.

Funding: This research was funded by the Italian Ministry of University and Research, in the framework of the Project "TECH4YOU" (Technologies for climate change adaptation and quality of life improvement), which was funded under the National Recovery and Resilience Plan (PNRR), Mission 4–Component 2–Investment 1.5 "Innovation ecosystems", by decree of the Ministry of University and Research on 23 June 2022, project code ECS 00000009.

Institutional Review Board Statement: Not applicable.

Informed Consent Statement: Not applicable.

Data Availability Statement: The raw data supporting the conclusions of this article will be made available by the authors on request.

Acknowledgments: This research was carried out in the framework of the project "TECH4YOU" (Technologies for climate change adaptation and quality of life improvement), which was funded under the National Recovery and Resilience Plan (PNRR), Mission 4–Component 2–Investment 1.5 "Innovation ecosystems", by decree of the Ministry of University and Research on 23 June 2022, project code ECS 00000009. The authors wish to thank EUMETSAT and the Aeronautica Militare Italiana for their support in having access to the MSG/SEVIRI data used in this work. During the preparation of this manuscript, the authors used ChatGPT 5.6 Sol and ChatGPT 5.5 (OpenAI) for language polishing only. The authors have reviewed and edited the output and take full responsibility for the content of this publication.

Conflicts of Interest: The authors declare no conflicts of interest.

Abbreviations

The following abbreviations are used in this manuscript:

POD	Proper Orthogonal Decomposition
SEVIRI	Spinning Enhanced Visible and Infrared Imager
MSG	Meteosat Second Generation
MIR	Middle Infrared
RST	Robust Satellite Techniques
RST-FIRES	Robust Satellite Techniques for FIRES
MODIS	Moderate Resolution Imaging Spectroradiometer
VIIRS	Visible Infrared Imaging Radiometer Suite
CS	Cosenza Province (Italy)
GMT	Greenwich Mean Time

References

1. Bowman, D.M.; Balch, J.K.; Artaxo, P.; Bond, W.J.; Carlson, J.M.; Cochrane, M.A.; d'Antonio, C.M.; DeFries, R.S.; Doyle, J.C.; Harrison, S.P.; et al. Fire in the Earth system. *Science* **2009**, *324*, 481–484.

2. Van Der Werf, G.R.; Randerson, J.T.; Giglio, L.; Van Leeuwen, T.T.; Chen, Y.; Rogers, B.M.; Mu, M.; Van Marle, M.J.; Morton, D.C.; Collatz, G.J.; et al. Global fire emissions estimates during 1997–2016. *Earth Syst. Sci. Data* **2017**, *9*, 697–720.
3. Jolly, W.M.; Cochrane, M.A.; Freeborn, P.H.; Holden, Z.A.; Brown, T.J.; Williamson, G.J.; Bowman, D.M. Climate-induced variations in global wildfire danger from 1979 to 2013. *Nat. Commun.* **2015**, *6*, 7537.
4. Zhai, G.; Dou, L.; Gu, Y.; Zhou, H.; Feng, L.; Jiang, L.; Dong, J.; Sun, J.; Li, H. From spark to suppression: An overview of wildfire monitoring, progression prediction, and extinguishing techniques. *Int. J. Appl. Earth Obs. Geoinf.* **2025**, *140*, 104600. https://doi.org/10.1016/j.jag.2025.104600.
5. Sung, T.; Kang, Y.; Im, J. Enhancing Satellite-Based Wildfire Monitoring: Advanced Contextual Model Using Environmental and Structural Information. *IEEE Trans. Geosci. Remote Sens.* **2024**, *62*, 4409516. https://doi.org/10.1109/TGRS.2024.3418475.
6. Abatzoglou, J.T.; Williams, A.P. Impact of anthropogenic climate change on wildfire across western US forests. *Proc. Natl. Acad. Sci. USA* **2016**, *113*, 11770–11775.
7. Brown, P.T.; Hanley, H.; Mahesh, A.; Reed, C.; Strenfel, S.J.; Davis, S.J.; Kochanski, A.K.; Clements, C.B. Climate warming increases extreme daily wildfire growth risk in California. *Nature* **2023**, *621*, 760–766.
8. Canadell, J.G.; Meyer, C.; Cook, G.D.; Dowdy, A.; Briggs, P.R.; Knauer, J.; Pepler, A.; Haverd, V. Multi-decadal increase of forest burned area in Australia is linked to climate change. *Nat. Commun.* **2021**, *12*, 6921.
9. Nematshahi, S.; Sohrabi, B.; Khodaei, A.; Arabnya, A.; Fan, R. Wildfire impact analysis on power system operation: A framework leveraging physics-based wildfire simulation and dynamic line rating. *Electr. Power Syst. Res.* **2026**, *252*, 112467. https://doi.org/10.1016/j.epsr.2025.112467.
10. Fernandez-Marcos, M.L. Potentially toxic substances and associated risks in soils affected by wildfires: A review. *Toxics* **2022**, *10*, 31.
11. Jin, Q.; Wang, W.; Zheng, W.; Innes, J.L.; Wang, G.; Guo, F. Dynamics of pollutant emissions from wildfires in Mainland China. *J. Environ. Manag.* **2022**, *318*, 115499.
12. Giglio, L.; Boschetti, L.; Roy, D.P.; Humber, M.L.; Justice, C.O. The Collection 6 MODIS burned area mapping algorithm and product. *Remote Sens. Environ.* **2018**, *217*, 72–85.
13. Chen, Y.; Morton, D.C.; Randerson, J.T. Remote sensing for wildfire monitoring: Insights into burned area, emissions, and fire dynamics. *ONE Earth* **2024**, *7*, 1022–1028. https://doi.org/10.1016/j.oneear.2024.05.014.
14. Giglio, L.; Descloitres, J.; Justice, C.O.; Kaufman, Y.J. An enhanced contextual fire detection algorithm for MODIS. *Remote Sens. Environ.* **2003**, *87*, 273–282.
15. Schroeder, W.; Oliva, P.; Giglio, L.; Csiszar, I.A. The New VIIRS 375 m active fire detection data product: Algorithm description and initial assessment. *Remote Sens. Environ.* **2014**, *143*, 85–96.
16. Zhang, D.; Huang, C.; Gu, J.; Hou, J.; Zhang, Y.; Han, W.; Dou, P.; Feng, Y. Real-time wildfire detection algorithm based on VIIRS fire product and Himawari-8 data. *Remote Sens.* **2023**, *15*, 1541.
17. Palumbo, I.; Samna, A.; Clerici, M.; Royer, A., Wildfire Monitoring with Satellite Remote Sensing in Support of Conservation. In *Satellite Remote Sensing for Conservation Action: Case Studies from Aquatic and Terrestrial Ecosystems*; Leidner, A.K., Buchanan, G.M., Eds.; Cambridge University Press: Cambridge, UK, 2018; p. 119–163.
18. Li, Z.; Fraser, R.; Jin, J.; Abuelgasim, A.A.; Csiszar, I.; Gong, P.; Pu, R.; Hao, W. Evaluation of algorithms for fire detection and mapping across North America from satellite. *J. Geophys. Res. Atmos.* **2003**, *108*, 4076. https://doi.org/10.1029/2001JD001377.
19. Giglio, L.; Schroeder, W.; Justice, C.O. The collection 6 MODIS active fire detection algorithm and fire products. *Remote Sens. Environ.* **2016**, *178*, 31–41.
20. Gautam, R.S.; Singh, D.; Mittal, A. An efficient contextual algorithm to detect subsurface fires with NOAA/AVHRR data. *IEEE Trans. Geosci. Remote Sens.* **2008**, *46*, 2005–2015.
21. Wooster, M.J.; Roberts, G.J.; Giglio, L.; Roy, D.P.; Freeborn, P.H.; Boschetti, L.; Justice, C.; Ichoku, C.; Schroeder, W.; Davies, D.; et al. Satellite remote sensing of active fires: History and current status, applications and future requirements. *Remote Sens. Environ.* **2021**, *267*, 112694. https://doi.org/10.1016/j.rse.2021.112694.
22. Vanhellemont, Q.; Neukermans, G.; Ruddick, K. Synergy between polar-orbiting and geostationary sensors: Remote sensing of the ocean at high spatial and high temporal resolution. *Remote Sens. Environ.* **2014**, *146*, 49–62. https://doi.org/10.1016/j.rse.2013.03.035.
23. Xu, W.; Wooster, M.J.; He, J.; Zhang, T. Improvements in high-temporal resolution active fire detection and FRP retrieval over the Americas using GOES-16 ABI with the geostationary Fire Thermal Anomaly (FTA) algorithm. *Sci. Remote Sens.* **2021**, *3*, 100016.
24. Wooster, M.J.; Roberts, G.; Freeborn, P.H.; Xu, W.; Govaerts, Y.; Beeby, R.; He, J.; Lattanzio, A.; Fisher, D.; Mullen, R. LSA SAF Meteosat FRP products–Part 1: Algorithms, product contents, and analysis. *Atmos. Chem. Phys.* **2015**, *15*, 13217–13239.
25. Roberts, G.; Wooster, M.; Lagoudakis, E. Annual and diurnal african biomass burning temporal dynamics. *Biogeosciences* **2009**, *6*, 849–866.

26. Filizzola, C.; Corrado, R.; Marchese, F.; Mazzeo, G.; Paciello, R.; Pergola, N.; Tramutoli, V. RST-FIRES, an exportable algorithm for early-fire detection and monitoring: Description, implementation, and field validation in the case of the MSG-SEVIRI sensor. *Remote Sens. Environ.* **2016**, *186*, 196–216.
27. Lumley, J.L. The structure of inhomogeneous turbulent flows. Atmospheric Turbulence and Radio Wave Propagation. In Proceedings of the International Colloquium, Moscow, Russia, 15–22 June 1965; pp. 166–178.
28. Holmes, P.; Lumley, J.L.; Berkooz, G.; Rowley, C.W. *Turbulence, Coherent Structures, Dynamical Systems and Symmetry*; Cambridge University Press: Cambridge, UK, 2012.
29. Berkooz, G.; Holmes, P.; Lumley, J.L. The proper orthogonal decomposition in the analysis of turbulent flows. *Annu. Rev. Fluid Mech.* **1993**, *25*, 539–575.
30. Alfonsi, G.; Restano, C.; Primavera, L. Coherent structures of the flow around a surface-mounted cubic obstacle in turbulent channel flow. *J. Wind Eng. Ind. Aerodyn.* **2003**, *91*, 495–511. https://doi.org/10.1016/S0167-6105(02)00429-4.
31. Alfonsi, G.; Primavera, L. The structure of turbulent boundary layers in the wall region of plane channel flow. *Proc. R. Soc. A Math. Phys. Eng. Sci.* **2007**, *463*, 593–612.
32. Vecchio, A.; Carbone, V.; Lepreti, F.; Primavera, L.; Sorriso-Valvo, L.; Veltri, P.; Alfonsi, G.; Straus, T. Proper orthogonal decomposition of solar photospheric motions. *Phys. Rev. Lett.* **2005**, *95*, 061102.
33. Veltri, P.; Vecchio, A.; Carbone, V. Proper orthogonal decomposition analysis of spatio-temporal behavior of renal scintigraphies. *Phys. Medica* **2010**, *26*, 57–70.
34. Ciardullo, G.; Primavera, L.; Ferrucci, F.; Carbone, V.; Lepreti, F. Study of Turbulence Associated with the Faraji Cyclone. *Climate* **2022**, *10*, 21.
35. Ciardullo, G.; Primavera, L.; Ferrucci, F.; Lepreti, F.; Carbone, V. New Investigation of a Tropical Cyclone: Observational and turbulence analysis for the Faraji Hurricane. *Remote Sens.* **2023**, *15*, 1383.
36. Ciardullo, G.; Primavera, L.; Ferrucci, F.; Lepreti, F.; Carbone, V. Remote Sensed Turbulence Analysis in the Cloud System Associated with Ianos Medicane. *Remote Sens.* **2026**, *18*, 602.